

Drop Deformation in Microconfined Shear Flow

Vincenzo Sibillo,¹ Gilberto Pasquariello,¹ Marino Simeone,¹ Vittorio Cristini,² and Stefano Guido^{1,*}

¹*Dipartimento di Ingegneria Chimica, Università di Napoli Federico II, Napoli 80125, Italy*

²*Department of Biomedical Engineering, University of California, Irvine, California 92697, USA*

(Received 12 March 2006; published 2 August 2006)

The deformation and breakup of a drop in an immiscible equiviscous liquid undergoing unbounded shear flow has been extensively investigated in the literature, starting from the pioneering work of Taylor. In this Letter, we address the case of microconfined shear flow, a problem which is relevant for microfluidics and emulsion processing applications. The main effects of confinement include complex oscillating transients and drop stabilization against breakup. In particular, very elongated drop shapes are observed, which would be unstable in the unbounded case and can be explained in terms of wall-induced distortion of the shear flow field. We show that wall effects can be exploited to obtain nearly monodisperse emulsions in microconfined shear flow.

DOI: [10.1103/PhysRevLett.97.054502](https://doi.org/10.1103/PhysRevLett.97.054502)

PACS numbers: 47.61.-k, 83.50.Ax, 83.80.Hj, 83.85.Ei

The deformation and breakup of a droplet in a continuous immiscible liquid phase under microconfined flow is a subject of growing interest in several applications. Examples are microfluidics technologies and emulsion processing [1]. In spite of its relevance, the current understanding of the effects of confinement on drop deformation, even in well-controlled flow fields, is rather limited, and the design issues concerning drop rheological behavior in microdevices are often addressed on an empirical basis [2]. In fact, starting from the pioneering work of Taylor [3], most of the literature on flow-induced drop deformation is devoted to the unbounded flow situation. The classical fluidodynamic problem investigated by Taylor is given by an isolated drop in a simple shear flow field, where the only intrinsic length scale is the undeformed drop radius a . In such a case (and with the further assumptions of Newtonian fluids and no surface active agents), the two nondimensional parameters governing drop shape and stability are the ratio of shear and interfacial stresses, expressed by the capillary number $Ca = a\eta\dot{\gamma}/\sigma$, where η is the continuous phase viscosity, $\dot{\gamma}$ is the shear rate, and σ is the interfacial tension, and the viscosity ratio λ between drop and continuous phase.

From the experimental side, Taylor analysis applies when the drop is located far enough from the confining surfaces of the flow device, so that the flow field can be taken, in fact, as unbounded. If such a condition is not satisfied, wall effects are known to influence the flow behavior of nearby drops. Thus, wall effects were found to elicit drop migration toward the center plane of a shear flow cell [4]. Experimental results of migration velocity [5,6] have been compared to predictions from small deformation theory [5,7] and to numerical simulations [8], and good agreement was found, except when the drop is in close proximity to the wall and for large values of λ .

More recently, an intriguing droplet-string transition has been found in concentrated polymer blends at a viscosity ratio of one when the size of the droplets becomes compa-

nable to the gap width between the shearing surfaces [9]. The transition was observed by shearing the sample between two parallel quartz disks and looking at the drops along the velocity gradient through stroboscopic optical microscopy. The strings are formed as a result of drop alignment into pearl necklace structures followed by drop coalescence, possibly due to wall-induced distortion of the velocity field. The effect of viscosity ratio on structure development, including coalescence and breakup, has also been addressed [10]. From the theoretical point of view, the hydrodynamic interaction between a drop in shear flow and the two confining walls has been analyzed at small deformations [11], but no comparison with experimental data has been presented so far. More recently, numerical simulations on two-dimensional wall-bounded shear flow of drop suspensions have been presented [12]; the consequences of dropping the third dimension, however, are not completely known. It so appears that a clear picture of drop deformation in confined shear flow is still lacking. In particular, no detailed information on the breakup dynamics is available. In this Letter, we report on the first systematic investigation of these issues at a viscosity ratio of one by using a high precision sliding plate device and show possible implications for operations involving microconfined shear flow.

The drops are observed along the vorticity direction of shear flow by using as parallel plates a couple of glass bars of square section (100 mm \times 50 mm \times 50 mm) [13]. Parallelism between the two plates is adjusted by a set of micrometric rotary and tilting stages (the residual error is around 20 μ m over a length of 10 cm). Shear flow at a constant shear rate $\dot{\gamma}$ is obtained by translating one of the plates at a constant speed with respect to the other through a computer-controlled motorized translating stage with micrometric precision setting. The microscope itself is also mounted on a separate motorized translating stage, which is used to keep the deforming drop within the field of view during motion. All the experiments are performed at

room temperature in a thermostated room. Isolated drops (with radius a ranging from 50 to 200 μm) are injected in the continuous phase, preliminarily loaded between the parallel plates, by a tiny glass capillary, fixed to a micro-manipulator for precise positioning. The drops are located in the middle of the gap between the sliding plates, and about halfway from the top and bottom glass slides to avoid further wall effects from these surfaces.

The continuous phase is a polybutene liquid exhibiting a fairly Newtonian behavior in the range of shear rates investigated ($0.01\text{--}0.03\text{ s}^{-1}$), with a viscosity of 83 Pas at room temperature and negligible first normal stress difference. The drop phase is prepared by mixing Newtonian silicone oils of different molecular weight in such proportions to match the polybutene viscosity. The interfacial tension of the pair of liquids is measured by a standard experimental procedure based on Taylor theory [14], and is 2.4 mN/m. Drop shape parameters, such as the axes L and B in the shear plane and the deformation parameter $D = (L - B)/(L + B)$, are measured by image analysis techniques (L and B are calculated as twice the maximum and minimum distance, respectively, between drop center and contour). Finally, buoyancy effects on the injected drop are found to be negligible on the time scale of the experiments, due to the high viscosities and the small density difference between the two liquids (ca. 0.08 g/cm^3) [9,10].

The experiments are started with an initial setting of the gap h between the confining plates high enough that no significant wall effects are anticipated. Several shear flow runs are then carried out at increasing values of $\dot{\gamma}$ (from one run to the other, the drop is allowed to retract back to the spherical shape at rest). This shear rate sweep is iterated at progressively lower gap settings by reducing the distance between the parallel plates (while maintaining the drop in the center of the gap) through a micrometric translating stage. The nondimensional gaps a/h investigated in this work range from 0.07 to 1 (the latter corresponds to the case of drop diameter twice the gap size). Images and deformation data from two representative runs at $\text{Ca} = 0.4$ and nondimensional gap $a/h = 0.07$ and 0.5 are shown in Fig. 1.

In the upper panel of Fig. 1 images taken at different times are presented for each run. The left sequence, which is referred to $a/h = 0.07$ ($h = 940\text{ }\mu\text{m}$), shows the typical shapes that are observed in the absence of wall effects. Starting from the spherical configuration at rest (1), the drop becomes more deformed and oriented in the flow direction (2)–(4) until a steady state shape is reached (5). Upon cessation of flow, drop deformation is relaxed (6) towards the equilibrium spherical shape. A striking difference in shape is found in the right image sequence, which corresponds to $a/h = 0.5$ ($h = 345\text{ }\mu\text{m}$; the walls have been highlighted in the images for the sake of clarity). In this case, starting again from the spherical configuration

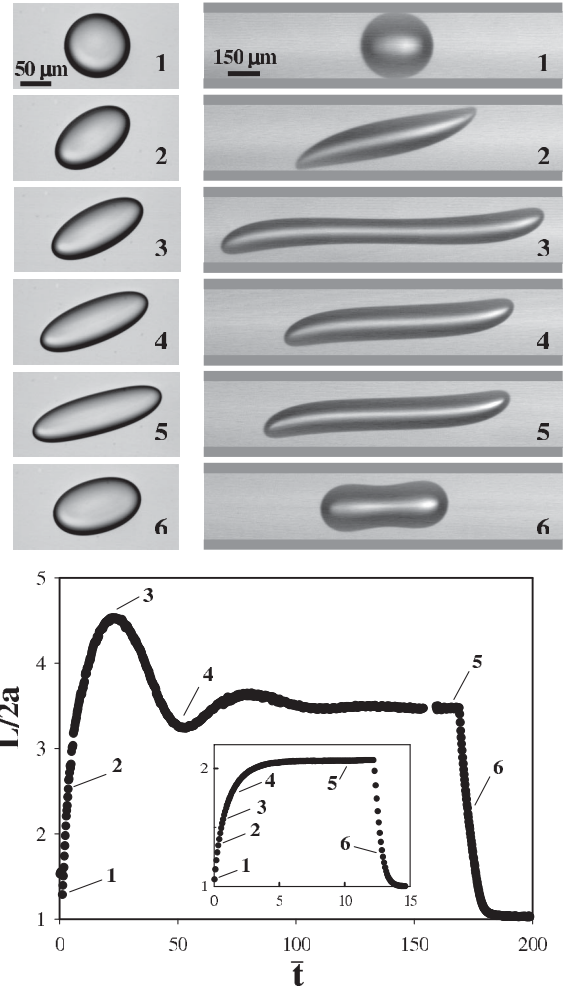


FIG. 1. Transient drop deformation at $\text{Ca} = 0.4$ and $a/h = 0.07$ (left sequence) and 0.5 (right sequence) as observed along the vorticity direction in a parallel flow apparatus. The viscosity ratio λ is equal to unity within experimental error.

(1), the steady state shape (5) is not attained monotonically, but drop deformation and orientation go through maxima (3) and minima (4) in a damped oscillatory fashion. Furthermore, at $a/h = 0.5$ the deformed drop is not ellipsoidal, as in the “unconfined” flow case ($a/h = 0.07$), but exhibits sigmoidal shapes, with pointed ends in the startup transient (2). As before, once the flow is stopped, drop relaxation towards the spherical configuration is observed, though with different retraction shapes (6). A quantitative representation of this trend is displayed in the bottom panel of Fig. 1, where the nondimensional drop axis $L/2a$ is plotted as a function of the nondimensional time \tilde{t} (given by the actual time multiplied by the shear rate $\dot{\gamma}$). For the sake of comparison, $L/2a$ versus time at $a/h = 0.07$ is shown in the inset in Fig. 1. It can be noticed that the stationary value of $L/2a$ is almost 1.7 times higher when $a/h = 0.5$ as compared to the unconfined case. In other words, the higher the confinement, the more extended is the drop shape at steady state. Furthermore, apart from the

complex transient behavior, which is missing for $a/h = 0.07$, the two cases differ in the time scale required to reach steady state conditions, which is an order of magnitude higher at $a/h = 0.5$. We found indeed that, at a given value of a/h , the startup transients became slower and slower with increasing Ca until it was not possible anymore to reach steady state within the total travel allowed by the apparatus.

In the small to moderate deformation regime, analytical expressions of drop deformation in confined shear flow have been derived by Shapira and Haber [11] based on Lorentz's reflection method. The resulting first-order corrections for wall effects show that drop shape, as calculated by Taylor [3], is not altered with respect to unbounded shear flow, only the magnitude of deformation is increased. A comparison of these predictions for two-wall effects with experimental data, which is not available at present in the literature, is here presented in Fig. 2, where the deformation parameter is plotted as a function of a/h for $Ca = 0.1, 0.2$, and 0.3 .

As shown before, at each value of Ca , drop deformation increases with a/h , i.e., by reducing the gap between the plates. As a matter of fact, the agreement between theory and predictions is remarkable, especially at the lower values of Ca , where small deformation theory is expected to hold. The corresponding stationary drop shapes for $Ca = 0.1$ are shown in the upper panel in Fig. 2, and it is interesting that even at the higher values of a/h , where distortions from the quasiellipsoidal shape are clearly visible, the agreement with theory is still quite satisfactory. This behavior is in line with the finding that Taylor predictions for D are in good agreement with experimental data up to drop deformations well beyond the range of validity of the small deformation theory, even though the

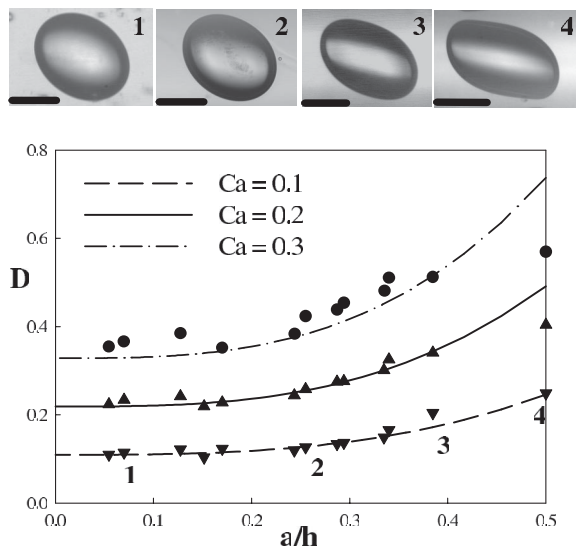


FIG. 2. Comparison between experimental data and the predictions of Shapira and Haber [11] at $Ca = 0.1, 0.2$, and 0.3 .

observed drop shape is quite different from the predicted one [14]. The Shapira and Haber predictions are still in good agreement with data at values of $Ca = 0.2$ and 0.3 , except when the drop gets too close to the wall (see the last point at $a/h = 0.5$), where the reflection analysis is expected to fail.

As a consequence of the increased drop deformation at reduced gap size, highly elongated shapes, which would be unstable in the unbounded case (see next paragraph), are observed at steady state in confined shear flow. Furthermore, the deformed drop is more oriented along the flow direction in the latter case. These trends are emphasized when drop diameter is greater than gap size (i.e., when $a/h > 0.5$). The stabilization of elongated drop shape can be explained in terms of wall-induced distortion of the shear flow field. Small wall separations, indeed, increase the amount of rigid-body rotation in the flow with respect to simple shear and thus result in nearly closed flow streamlines. We have performed boundary-integral simulations [data not shown, see [15] for details] that demonstrate that this confines the droplet to rotating within the closed streamlines, in contrast to the no-wall case, in which shear flow streamlines are open and droplet deformation can be unbounded thus leading to breakup. The major consequence of this phenomenon is that higher droplet deformations are stable and breakup is hampered.

Another remarkable aspect of confined drop deformation is related to the critical behavior at breakup. We found that both the critical capillary number and the breakup time are somehow increased with respect to the unbounded case. An example is shown in Fig. 3, where selected images illustrating drop shape evolution with time are presented at

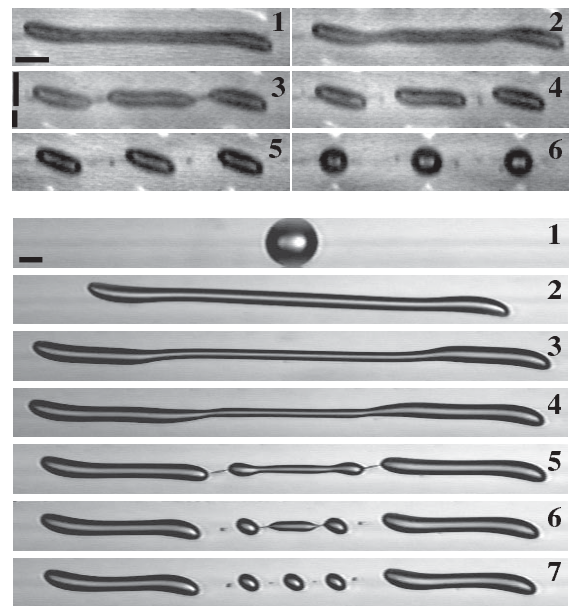


FIG. 3. Drop breakup dynamics at $Ca = 0.46$ and $a/h = 0.7$ (top sequence, scale bar = $100 \mu\text{m}$) and $Ca = 0.5$ and $a/h = 1$ (bottom sequence, scale bar = $150 \mu\text{m}$).

$Ca = 0.46$ for $a/h = 0.35$ (top sequence) and $Ca = 0.5$ and $a/h = 0.5$ (bottom sequence). In the slightly supercritical conditions at $Ca = 0.46$ of the top sequence in Fig. 3, the breakup dynamics is characterized by drop elongation followed by pinch-off at the ends of the neck region (at $L/2a = 6$). The fragments generated upon breakup are three main daughter drops and two minor satellites in between them (image 5). An interesting feature of this breakup mode is that the central daughter drop is just slightly different (5% in radius) than the two daughter drops at the ends. Such behavior is at variance with the unbounded case, where the central fragments are smaller than the two main daughter drops at the ends. This suggests that confined shear flow could be exploited to generate quasi monodisperse emulsions by controlled breakup under near critical conditions. It can be noticed that the capillary number in the top sequence in Fig. 3 is slightly higher than the critical value for breakup in unbounded shear flow at $\lambda = 1$, which is ca. 0.43 [16]. The nondimensional breakup time, however, is more than twice the corresponding value for unbounded flow [17], thus confirming the slowing down of drop deformation kinetics induced by microconfined flow. Furthermore, the nondimensional drop axis at breakup is also higher than the corresponding value in unbounded shear.

The effect of confinement becomes more pronounced when drop diameter approaches gap size. At $a/h = 0.5$, the deformed drop tends to a stable stationary shape, following a transient with damped oscillations, still at $Ca = 0.48$, which would correspond to a supercritical condition (i.e., leading to breakup) in unbounded shear. At $Ca = 0.5$, as in the bottom sequence of Fig. 3, no oscillations are observed since the drop keeps elongating up to a point where pinch off takes place (at $L/2a = 10$). The conical neck left behind retracts forming a bulbous part, where a further breakup event takes place. This is a common behavior in free-surface flows, such as jet breakup [18]. The breakup time, which is ca. 65, is more than 3 times higher compared to the value for unbounded flow at the same value of Ca [ca. 20, [17]]. Overall, nine fragments are generated upon breakup, including two larger daughter drops, three main, and four smaller satellites (image 5). It so appears that, at a given Ca , breakup occurs at a higher elongation and at longer times in the confined case due to the stabilizing effect of the walls, thus generating more fragments compared to unbounded flow.

In conclusion, we have described deformation and breakup of an isolated drop undergoing two-phase confined shear flow in a precision sliding plate apparatus at a viscosity ratio of one. Wall effects act to stabilize elongated drop shapes, which would be otherwise unstable in the unbounded case, by confining the drop to rotate within

closed streamlines. This feature could be relevant for the production of elongated microstructures, which is an important technological issue in several applications, such as food processing, where the particle shape can be “frozen” by gelation. Another possible application of the results shown in this work is the generation of quasimonodisperse emulsions by controlled breakup of fluid droplets. By proper selection of flow geometry and fluid properties, daughter droplets of similar size can be obtained by breakup close to the critical conditions.

*Email address: stefano.guido@unina.it

- [1] H. Stone, A. Stroock, and A. Ajdari, *Annu. Rev. Fluid Mech.* **36**, 381 (2004).
- [2] V. Cristini and Y.-C. Tan, *Lab Chip* **4**, 257 (2004).
- [3] G.I. Taylor, *Proc. R. Soc. A* **138**, 41 (1932); **146**, 501 (1934).
- [4] A. Karnis and S.G. Mason, *J. Colloid Interface Sci.* **24**, 164 (1967).
- [5] J.R. Smart and D.T. Leighton, *Phys. Fluids A* **3**, 21 (1991).
- [6] P. C. H. Chan and L. G. Leal, *Int. J. Multiphase Flow* **7**, 83 (1981); M. R. King and D. T. Leighton, *Phys. Fluids* **13**, 397 (2001); S. D. Hudson, *Phys. Fluids* **15**, 1106 (2003).
- [7] C. E. Chaffey, H. Brenner, and S. G. Mason, *Rheol. Acta* **4**, 64 (1965); P. C. H. Chan and L. G. Leal, *J. Fluid Mech.* **92**, 131 (1979); T. Imaeda, *Physica (Amsterdam)* **285A**, 306 (2000).
- [8] W. S. J. Uijttewaal, E. J. Nijhof, and R. M. Heethaar, *Phys. Fluids A* **5**, 819 (1993); M. R. Kennedy, C. Pozrikidis, and R. Skalak, *Comput. Fluids* **23**, 251 (1994); W. S. J. Uijttewaal, and E. J. Nijhof, *J. Fluid Mech.* **302**, 45 (1995).
- [9] K. B. Migler, *Phys. Rev. Lett.* **86**, 1023 (2001); J. A. Patak and K. B. Migler, *Langmuir* **19**, 8667 (2003).
- [10] A. Vananroye, P. V. Puyvelde, and P. Moldenaers, *Langmuir* **22**, 2273 (2006); **22**, 3972 (2006).
- [11] M. Shapira and S. Haber, *Int. J. Multiphase Flow* **16**, 305 (1990).
- [12] X. Li and C. Pozrikidis, *Int. J. Multiphase Flow* **26**, 1247 (2000); J. Lee and C. Pozrikidis, *Comput. Fluids* **35**, 43 (2006).
- [13] S. Guido and M. Simeone, *J. Fluid Mech.* **357**, 1 (1998).
- [14] S. Torza, R. G. Cox, and S. G. Mason, *J. Colloid Interface Sci.* **38**, 395 (1972); S. Guido and M. Villone, *J. Rheol. (N.Y.)* **42**, 395 (1998).
- [15] V. Cristini, J. Blawdziewicz, and M. Loewenberg, *J. Comput. Phys.* **168**, 445 (2001).
- [16] V. Cristini, J. Blawdziewicz, and M. Loewenberg, *Phys. Fluids* **10**, 1781 (1998).
- [17] V. Cristini, S. Guido, A. Alfani, J. Blawdziewicz, and M. Loewenberg, *J. Rheol. (N.Y.)* **47**, 1283 (2003).
- [18] J. Eggers, *Rev. Mod. Phys.* **69**, 865 (1997).